Chapter 5

A Continuous Beam Scanning and Beamwidth Tuning Microstrip Cross Parasitic Antenna with Polarization Reconfiguration

5.1 Introduction

The pattern reconfigurable antenna designs presented in Chapter 3 and Chapter 4 are linearly polarized. The CP antennas have several advantages as compared with LP antennas. The benefits of CP antennas include insensitivity to multipath reflection, suppression of polarization losses and immunity to Faraday rotation effects [2]. After careful investigation, it is found that the majority of the pattern RA designs reported are linearly polarized. Once the antenna design is optimized for one polarization in one direction, scanning the main beam while keeping the sense of polarization remains a challenge. The primary concern in CP beam scanning antennas is to achieve AR below 3 dB for all the scanning angles. Several studies on scanning the CP radiated beam using microstrip Yagi principle has been reported in the literature. However, in those designs, polarization reconfiguration is not achieved and the main beam is scanned with only one polarization either RHCP [44, 115, 116, 119] or LHCP [117, 118]. It is also observed that the earlier reported RA designs are not able to provide independent pattern and

polarization reconfiguration, which significantly limits diversity provided by the compound RA [14, 120–129, 143, 144].

In this chapter, RA design is proposed to realize independent pattern and polarization reconfiguration along with beamwidth reconfiguration at an operating frequency of 2.45 GHz. The RA design achieving independent reconfiguration of all the three parameters pattern, beamwidth and polarization in a single antenna structure is not yet reported in the literature. This antenna consists of a dual coaxial-feed square-shaped driven patch surrounded by four tunable parasitic elements. Each tunable parasitic element consists of a square-shaped slot loaded with four varactor diodes. Continuous beam scanning in the elevation plane is achieved by utilizing mutual coupling between the driven and tunable parasitic elements. The RFN is designed and developed to produce two orthogonal LP (LVP, LHP) and CP (LHCP, RHCP) operating states. In LP operating mode, main beam of the antenna is continuously scanned in the elevation plane from θ = 0° to 11°, 0° to 32°, and 0° to 40° in ϕ = ±0°, ±45°, and ±90° plane respectively. In CP operating mode, the radiated beam is continuously scanned from 0° to 30° in ϕ = ±0°, ±45° and ±90° plane respectively with AR less than 3 dB in all the beam scanning directions. In addition to this, the 3-dB beamwidth of this antenna can be continuously tuned in E-plane, H-plane, and both E-plane and H-plane with LVP and LHP from 66° to 152°, 60° to 108°, and 78° to 120° respectively.

This chapter is organized as follows: Section 5.2 presents a geometrical design of the proposed pattern and polarization RA. This section also describes the design and operating principle of RFN, which is to produce LVP, LHP, LHCP, and RHCP operating states. The simulated and measured results are discussed in Section 5.3. In the end, the performance of the proposed antenna is compared with the other similar types of antennas. Summary of this chapter is presented in Section 5.4.

5.2 Antenna Design

This section presents the proposed antenna design and details associated with the DC biasing circuit. Different techniques used to achieve CP in microstrip antennas are also discussed. Performance of the single-feed CP beam scanning antenna is compared with the dual-feed antenna configuration. Simulated and measured results of the 3-dB quadrature hybrid coupler and RFN are also presented.

5.2.1 Antenna Configuration

Figure 5.1 shows front and back view of the pattern and polarization RA. This antenna consists of a dual-feed square-shaped driven element and four varactor loaded tunable parasitic elements P1, P2, P3 and P4 placed on each side of the driven element. Geometrical parameters of the antenna are as follows (in mm): L = 28.9, L_1 = 7.5, L_2 = 8.5, W_1 = 1, g = 3, k = 8.95, L_h = 16, W_h = 0.5 and L_g = W_g = 140. The length of the driven and tunable parasitic elements is L. Each tunable parasitic element consists of a square-shaped slot loaded with four varactor diodes. The tunable parasitic elements are isolated from the driven element by a spacing of g. The antenna is designed using FR4 substrate with ϵ_r = 4.3, h = 1.6 mm and $\tan\delta$ = 0.02. DC voltage to the cathode terminal of varactor diodes is applied using metallic vias V1, V2, V3, and V4 through Coilcraft RF choke coil. The anode terminal of the varactor diodes is grounded using metallic vias V5, V6, V7, and V8 which are connected to the negative terminal of the power supply.

5.2.2 Beam Scanning with Circular Polarization

To generate CP in microstrip patch antennas, two orthogonal modes should be excited with equal amplitude and phase quadrature. This can be attained by employing single-feed or dual-feed excitation [161]. In single-feed antennas, CP is generated by modifying the square-shaped microstrip patch antenna. The dual-feed antennas need an external feeding network consisting of a power divider and hybrid coupler to obtain equal amplitude and 90° phase difference between the two ports. In this section, the effects of single-feeding and dual-feeding method on CP beam scanning characteristics are discussed in detail. The advantages and limitations of both techniques are described. In the end, reasons are given for the selection of dual-feed antenna configuration to design the proposed pattern and polarization RA.

5.2.2.1 Single-Feed Configuration

A single-feed RHCP antenna is designed by making corner truncation in the ground plane. Figure 5.2 shows the front and back view of the antenna. Length of the square-shaped patch is L, and the overall size of the antenna is $L_g \times W_g$. The corner truncated length t and feeding point position k is optimized to obtain good CP performance at an operating frequency of 2.45 GHz. Optimized dimensions of the antenna are as follows (in mm): L = 29, k = 7, t = 8, and L_g = W_g = 50. In this design, the polarization reconfiguration can be achieved by adding PIN diodes in the truncated area. To obtain all the polarization states, four corner truncations are needed on the ground plane.

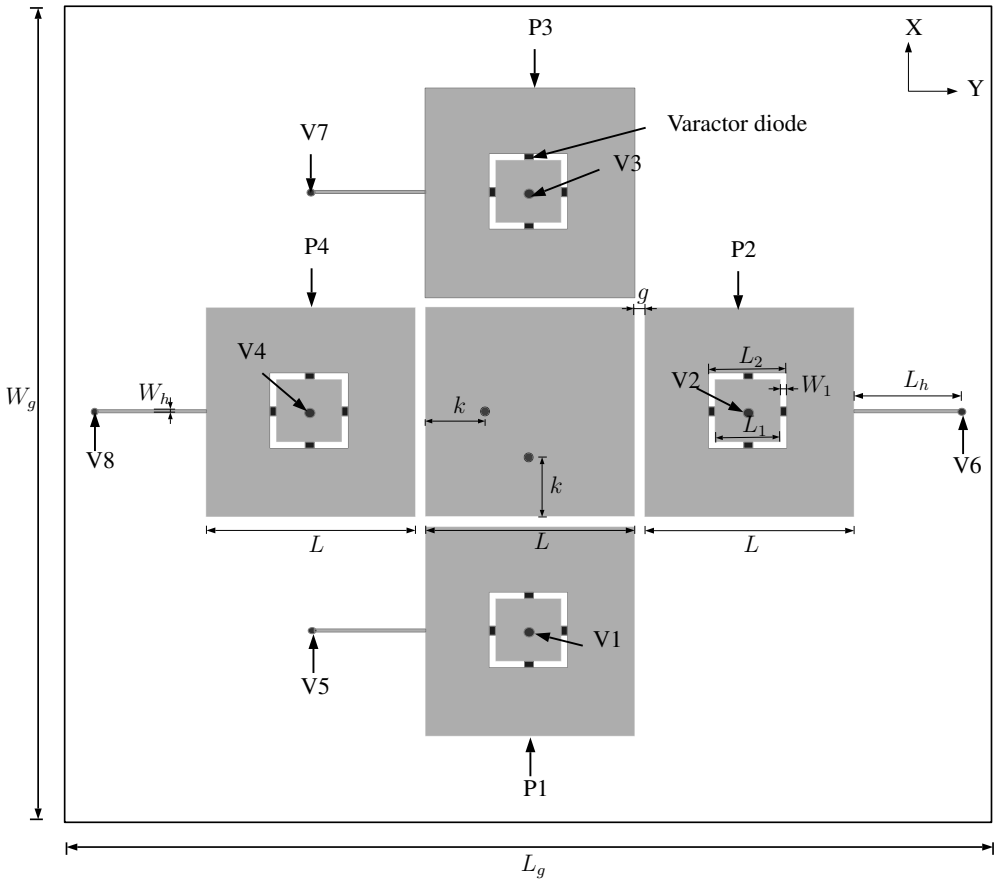

(a)

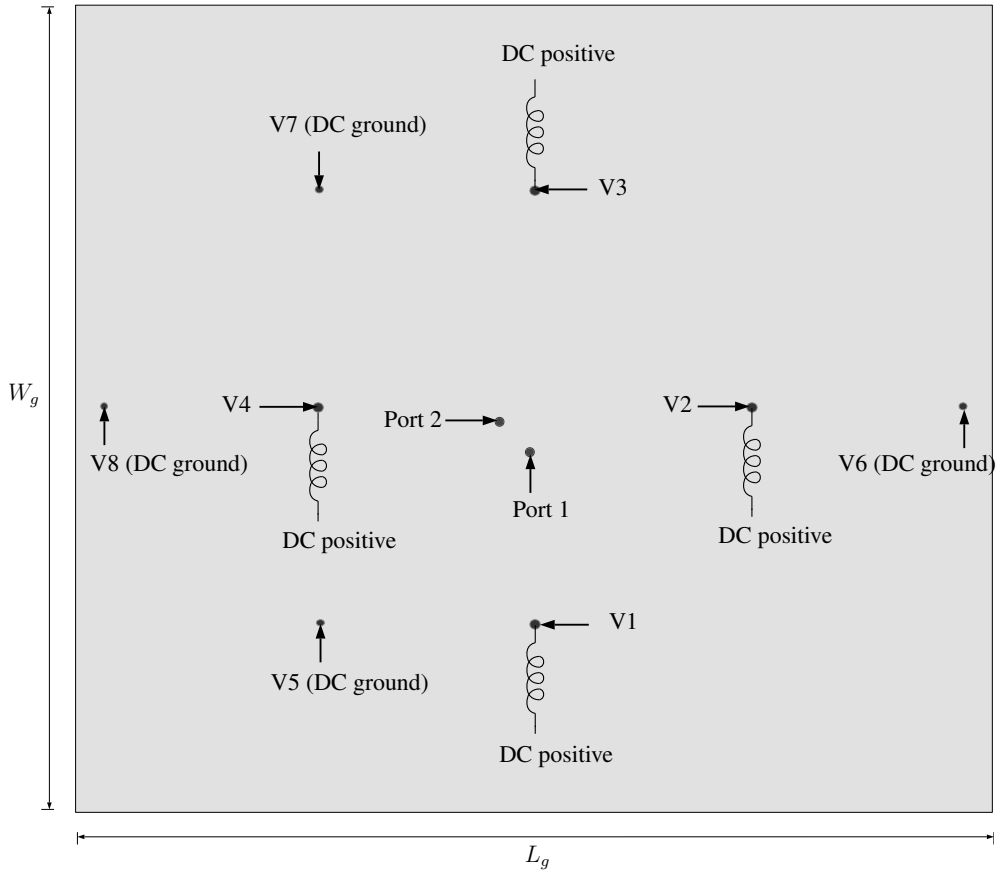

(b)

Figure 5.1. Geometrical design of the pattern and polarization RA (a) Front view and (b) Back view.

The polarization mode of the antenna can be changed by controlling a switching state of the PIN diode. Polarization reconfiguration can also be accomplished by making corner truncations on the radiating patch. However, this approach needs a separate RF and DC isolation circuit on the radiating patch, which complicates the overall biasing circuit design.

The simulated result displayed in Figure 5.3 shows that this antenna achieves -10 dB impedance bandwidth from 2.38 to 2.52 GHz (5.72%). In both the principal planes, broadside radiation is obtained with a gain of 3.50 dBic. The cross-polarized component in the broadside direction is found to be less than -20.65 dB. Figure 5.4 shows simulated AR results obtained in the xz-plane and yz-plane. The 3-dB AR beamwidth in the xz-plane and yz-plane is in the range of $-90°$ to $101°$ and $-86°$ to $78°$ respectively. The 3-dB AR bandwidth in both the planes is 2.427 to 2.457 GHz (1.23%). Thus, by making corner truncation in the square-shaped patch -10 dB impedance bandwidth of the antenna increases. However, the overlapped bandwidth is extremely narrow and is limited by the 3-dB AR bandwidth.

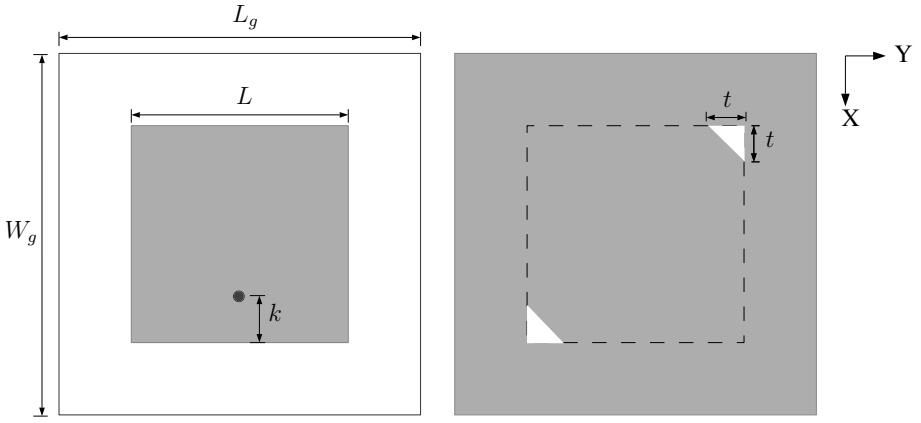

Figure 5.2. Geometrical design of the single-feed square-shaped antenna with corner truncation in the ground plane (a) Front view and (b) Back view.

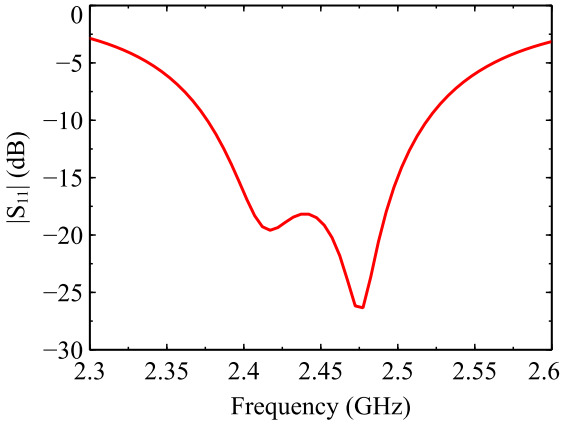

Figure 5.3. Simulated reflection characteristics of the corner truncated single-feed patch antenna.

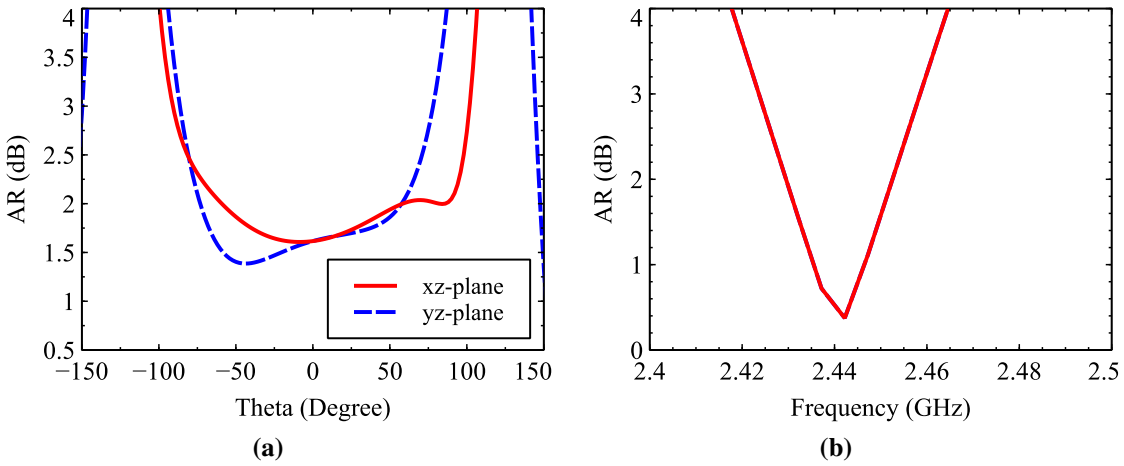

Figure 5.4. Simulated radiation characteristics in the xz-plane and yz-plane (a) AR beamwidth and (b) AR bandwidth.

The effect of single-feed patch on CP beam scanning characteristics is analyzed by placing one tunable parasitic element in the H-plane at a distance of 3 mm. Here, CP is obtained by making corner truncation in the ground plane, and beam scanning is achieved by utilizing mutual coupling between the antenna elements. Figure 5.5 shows the geometrical design for the proposed configuration. Optimized dimensions of the antenna are as follows (in mm): L = 29, L_1 = 7.5, L_2 = 8.5, k = 7, g = 3, L_g = 120 and W_g = 60. The tunable parasitic element consists of a square-shaped slot loaded with two varactor diodes. The capacitance of the varactor diode is varied from 0.84 to 3.95 pF. Figure 5.6 shows the simulated reflection characteristics, and it can be observed that the -10 dB impedance bandwidth is from 2.39 to 2.51 GHz (4.90%). Main beam of the antenna is continuously scanned in the elevation plane from $-22°$ to 18°, as the capacitance is varied from 0.84 to 3.95 pF with gain variation from 3.11 to 1.37 dBic. The simulated CP beam scanning characteristics are shown in Figure 5.7. Figure 5.8 presents simulated AR results for the capacitance range from 0.84 to 3.95 pF at an operating frequency of 2.45 GHz. The results are observed in the main beam scanned direction for each capacitance value. The AR is found to be less than 3 dB for all the capacitance values and is in the range of 2.83 to 0.56 dB. The overall 3-dB AR bandwidth is from 2.446 GHz to 2.451 GHz (0.2%). In conclusion, for the proposed antenna configuration main beam can be continuously scanned in the elevation plane with good CP performance at 2.45 GHz. However, the overall -10 dB and 3-dB AR bandwidth is found to be extremely narrow.

The earlier presented two-element design is further extended to form a cross antenna structure consisting of a single-feed driven element and four tunable parasitic elements. Each tunable parasitic element is composed of a square-shaped slot with two varactor diodes. Here, the beam scanning performance is analyzed in yz-plane (ϕ = 90°) by varying the capacitance of tunable

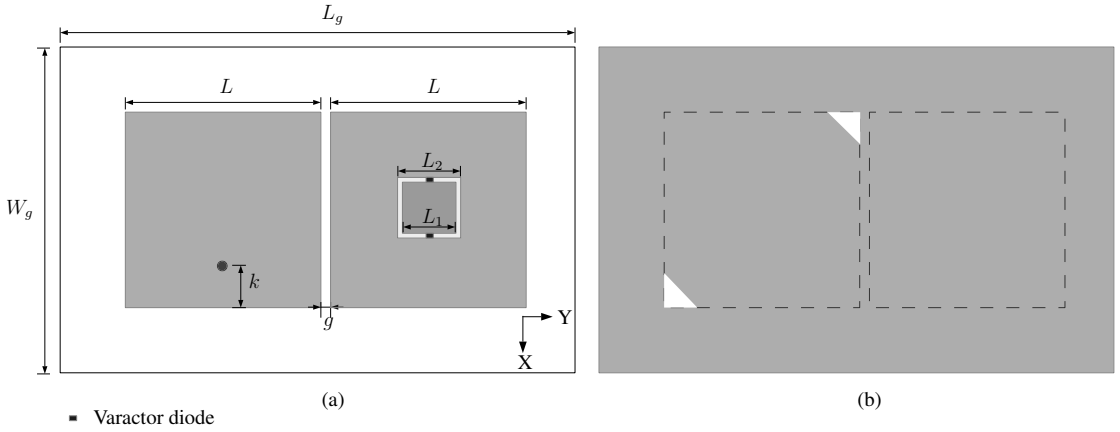

Figure 5.5. Geometrical design of the single-feed driven element with corner truncation on the ground plane and one tunable parasitic element (a) Front view and (b) Back view.

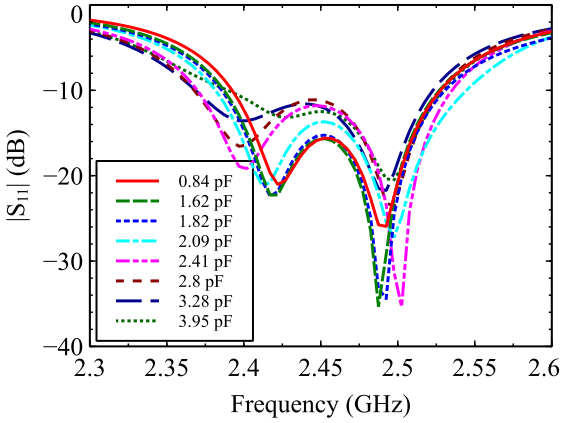

Figure 5.6. Simulated reflection characteristics of the single-feed driven element with corner truncation on the ground plane and one tunable parasitic element.

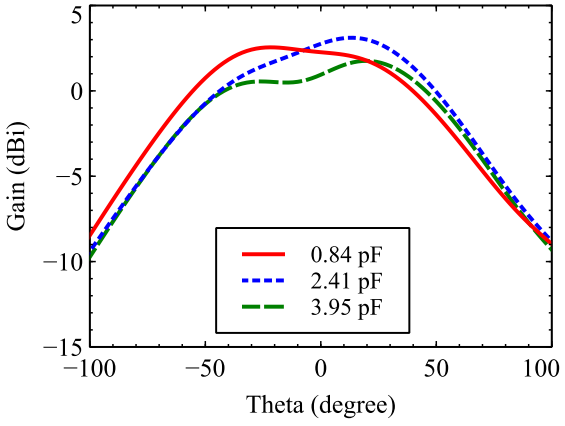

Figure 5.7. Simulated CP beam scanning characteristics of the single-feed driven element with corner truncation on the ground plane and one tunable parasitic element.

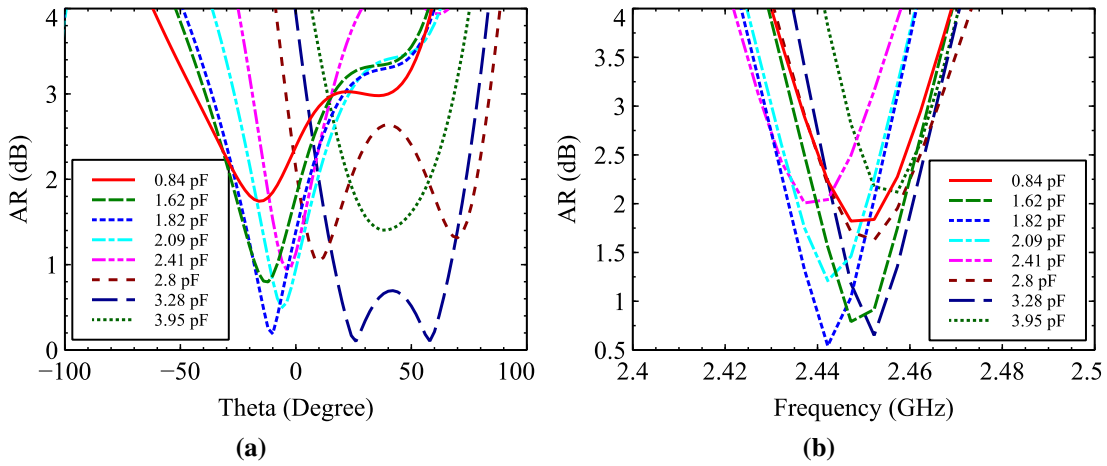

Figure 5.8. Simulated radiation characteristics of the single-feed driven element with corner truncation on the ground plane and one tunable parasitic element (a) AR beamwidth and (b) AR bandwidth.

parasitic element P2 placed in the H-plane from 1.62 to 5.08 pF. The capacitance of tunable parasitic element P4 is fixed at 0.84 pF to have good reflector characteristics. Capacitance of the tunable parasitic elements P1 and P3 placed in the E-plane is fixed at 1.82 pF. Figure 5.9(a) shows the simulated reflection characteristics for all the capacitance values. This antenna shows good impedance matching for all the capacitance values with -10 dB impedance bandwidth from 2.37 to 2.52 GHz. As the capacitance of tunable parasitic element P2 is varied from 1.62 to 5.08 pF, the main beam is continuously scanned from 4° to 28° with a gain variation from -1.90 to 0.89 dBic. Figure 5.9(b) shows simulated AR beamwidth characteristics at 2.45 GHz. It can be seen that the AR is less than 3 dB in the main beam scanned direction for the capacitance values 1.62 pF and 1.82 pF and is found to be 1.11 dB and 1.78 dB, respectively. The 3-dB AR beamwidth for these capacitance values ranges from $-20°$ to 36° and $-12°$ to 36° respectively. However, it is worth mentioning that the overall CP performance gets degraded as the main beam moves away from the broadside direction, and AR is found to be greater than 3 dB. For the capacitance range from 2.09 to 5.08 pF, the AR is in the range of 3.39 to 7.44 dB.

5.2.2.2 Dual-Feed Configuration

In this section, the effect of dual-feed configuration on the CP beam scanning characteristics is analyzed. First, a dual-feed square-shaped antenna is simulated in HFSS. Figure 5.10 shows the geometrical design of the dual-feed square-shaped CP antenna. Dimensions of the antenna are as follows (in mm) : $L = 28.5$, $k = 6$ and $L_g = W_g = 50$. Here, port 1 and port 2 is excited with $1\angle 0°$ and $1\angle 90°$ respectively to produce RHCP radiation.

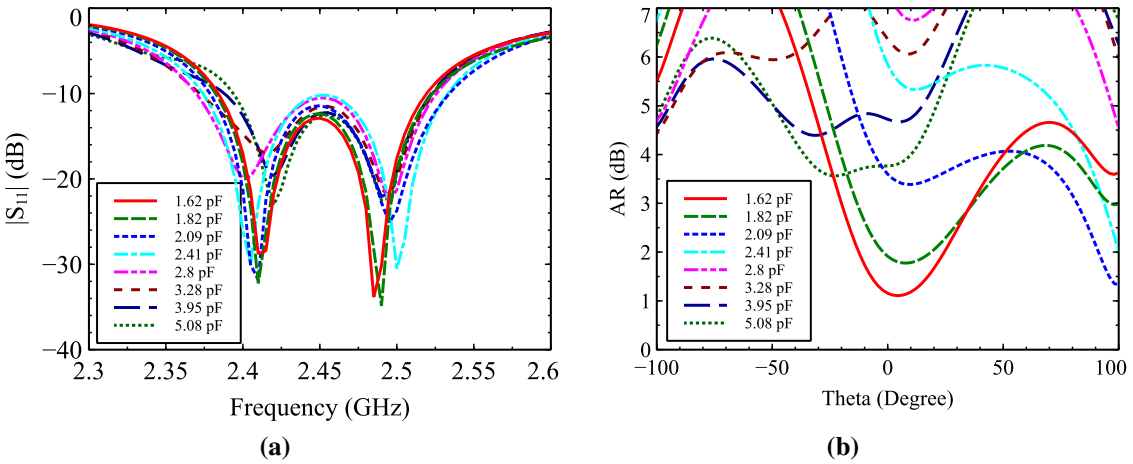

Figure 5.9. Simulated results in ϕ = 90° plane for single-feed driven element with corner truncation on the ground plane and four tunable parasitic elements (a) Reflection characteristics and (b) AR beamwidth.

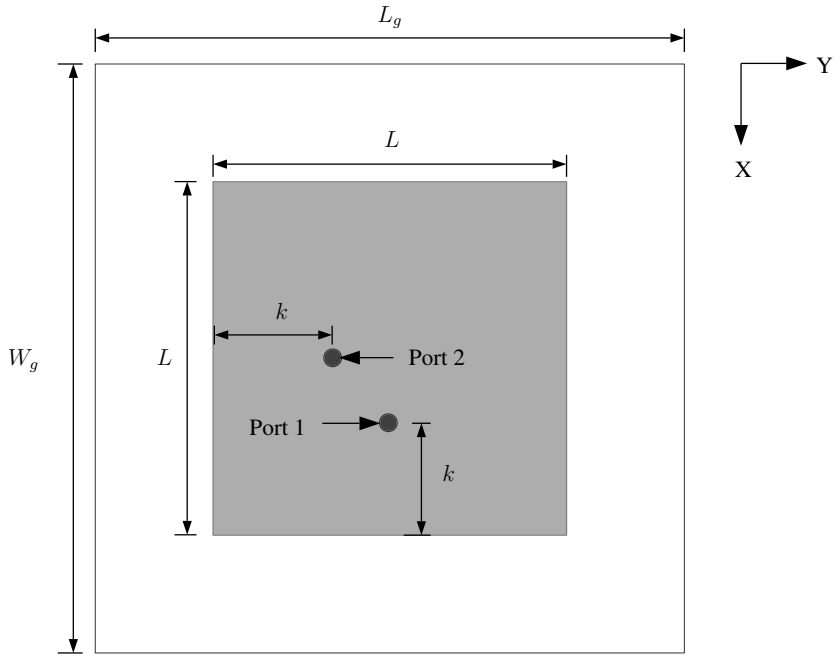

Figure 5.10. Geometrical design of the dual-feed square-shaped patch antenna.

This antenna achieves good reflection characteristics with −10 dB impedance bandwidth from 2.42 to 2.49 GHz, as shown in Figure 5.11(a). From Figure 5.11(b) it can be seen that the isolation between the two ports is found to be −35 dB at 2.45 GHz. The simulated radiation pattern in both the principal planes shows broadside radiation characteristics with a gain of 3.38 dBic, as shown in Figure 5.12. Figure 5.13 shows simulated AR results in the xz-plane and yz-plane. The 3-dB AR beamwidth in he xz-plane and yz-plane is −88° to 98° and −98° to 96° respectively. The 3-dB AR bandwidth in both the principal planes in the broadside direction is found to be from 1.25 to 2.94 GHz. Overall bandwidth in the dual-feed CP antenna is limited by the −10 dB impedance bandwidth.

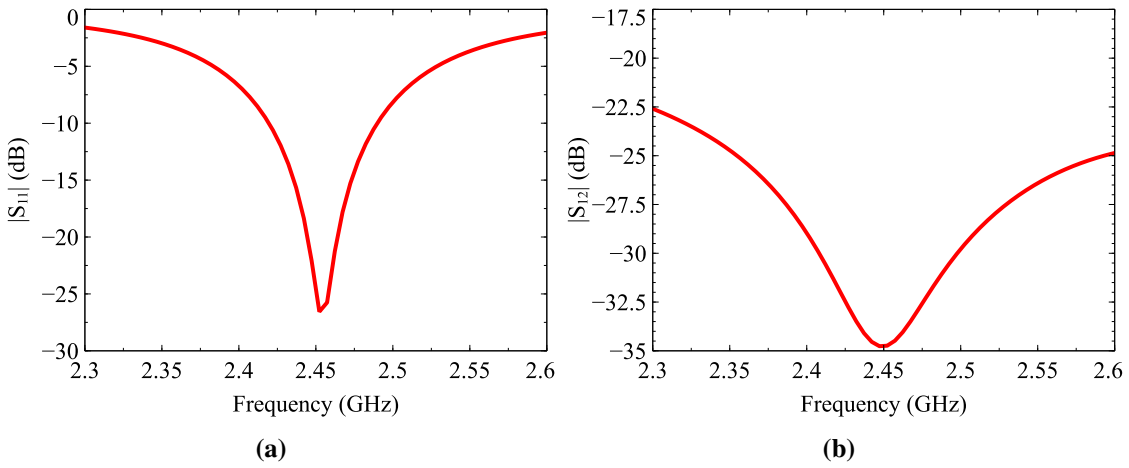

Figure 5.11. Simulated reflection characteristics of the dual-feed square-shaped patch antenna (a) $|S_{11}|$ and (b) $|S_{12}|$.

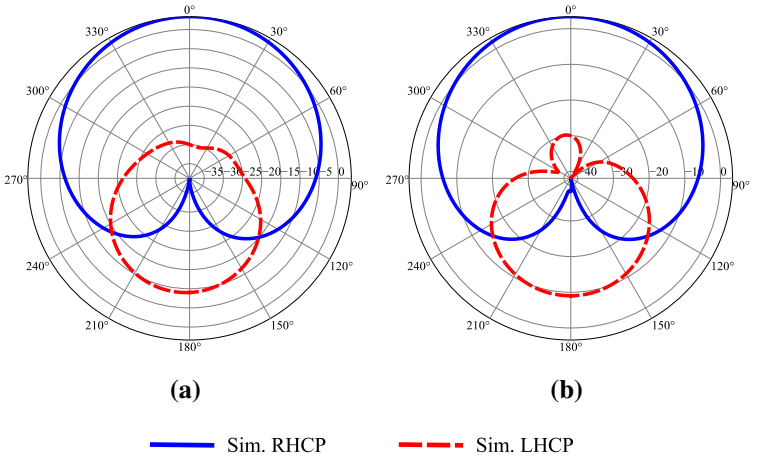

Figure 5.12. Simulated radiation pattern for the dual-feed CP antenna (a) xz-plane and (b) yz-plane.

Figure 5.14 shows a geometrical design of the dual-feed driven element with one tunable parasitic element. The tunable parasitic element is composed of a square-shaped slot loaded with four

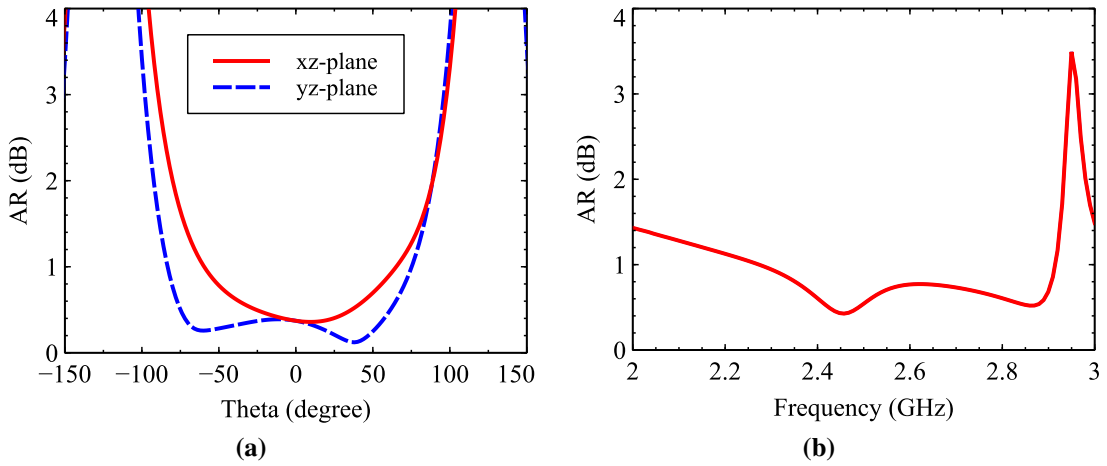

Figure 5.13. Simulated radiation characteristics of the dual-feed CP antenna (a) AR beamwidth and (b) AR bandwidth.

varactor diodes. It is observed that to obtain CP beam scanning in dual-feed antenna configuration, varactor diodes need to be placed along each coaxial-feed. Here, a square-shaped slot is selected since it provides symmetrical slot locations to place two varactor diodes along both the feed directions. The square-shaped varactor loaded tunable parasitic element shows dual-band characteristics, and hence its effective electrical size can be changed with respect to the driven element. Table 5.1 summarizes detailed simulated dual-band characteristics for the capacitance range from 0.84 to 5.08 pF. The reflector and director characteristics of the tunable parasitic element are used to achieve continuous beam scanning. Dimensions of this antenna are as follows (in mm): $L = 28.9$, $L_1 = 7.5$, $L_2 = 8.5$, $k = 8.95$, $g = 3$, $L_g = 120$ and $W_g = 60$. The performance of this antenna is analyzed for the capacitance range from 0.84 to 5.08 pF. The simulation result shows that this antenna maintains impedance matching for all the capacitance values with an overall -10 dB impedance bandwidth from 2.42 to 2.47 GHz. Detailed simulated results are summarized in Table 5.2. Main beam of the antenna is continuously scanned from -14° to 24°, as the capacitance is varied from 0.84 to 5.08 pF. The AR in each beam scanned direction is found to be in the range of 1.02 to 1.92 dB. Gain of the antenna changes from 3.58 to 0.95 dBic over the beam scanning range. The overall 3-dB beamwidth coverage is from -57° to 58°. In conclusion, the dual-feed antenna with one tunable parasitic element shows the desired CP beam scanning performance for all the capacitance values. This antenna achieves AR less than 3 dB in all the beam scanning directions over a large bandwidth as compared to the corner truncated patch antenna. The single-feed corner truncated CP beam scanning cross parasitic antenna has an advantage of simple design. However, the overall bandwidth is narrow, and it is difficult to achieve good CP performance for all the scanning angles. The cross parasitic antenna designed using a dual-feed mechanism produces AR less than 3 dB in all the beam scanning directions for the entire

azimuth plane. However, complex RFN involving hybrid coupler and RF switches is required to obtain polarization reconfiguration. These guidelines are used to design a dual-feed reconfigurable cross parasitic antenna by placing four tunable parasitic elements around the driven element.

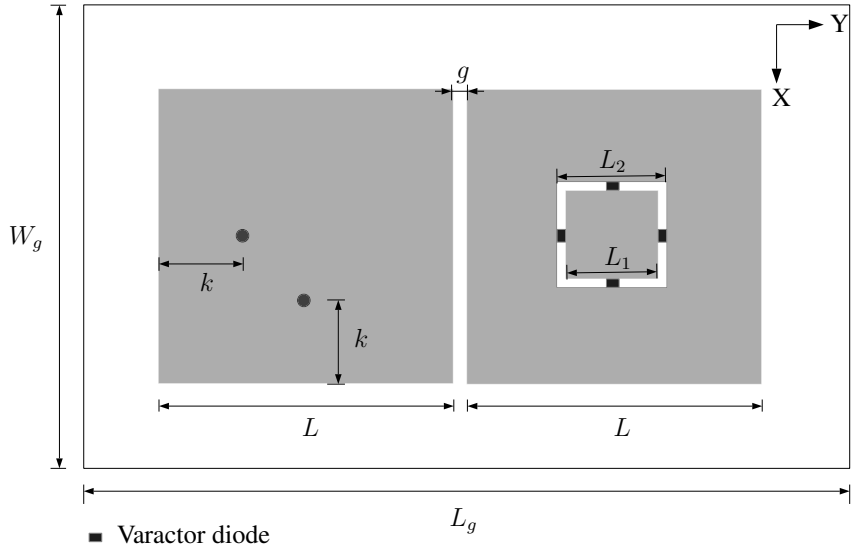

Figure 5.14. Geometrical design of the square-shaped dual-feed driven element with one tunable parasitic element.

Table 5.1. Dual-band characteristics of a coaxial-feed square-shaped patch with varactor loaded slot for capacitance range from 0.84 to 5.08 pF.

Capacitance (pF)	f_1 (GHz) $\lvert S_{11}\rvert$ (dB)	f_2 (GHz) $\lvert S_{11}\rvert$ (dB)
0.84	2.25 (−13.13)	3.52 (−11.72)
1.82	2.08 (−9.62)	2.66 (−1.46)
2.09	2.01 (−10.68)	2.57 (−4.03)
2.41	1.92 (−14.88)	2.52 (−7.56)
2.8	1.82 (−32.51)	2.49 (−12.72)
3.28	1.71 (−18.33)	2.46 (−18.28)
3.95	1.57 (−11.28)	2.44 (−25.30)
5.08	1.40 (−7.18)	2.42 (−24.46)

5.2.3 Reconfigurable Feeding Network

In this section, the operating mechanism of the RFN is discussed. Simulated and measured results of the 3-dB quadrature hybrid coupler and linear tapered feed line are also presented. Figure 5.15 shows a block diagram of the proposed RFN used to produce LP and CP reconfiguration. The RFN consists of a 3-dB quadrature hybrid coupler, one Single Pole Four Throw (SP4T) switch, and two Single Pole Double Throw (SPDT) switches. Input to the RFN (port 1) is applied using a 50 Ω end-launched SMA connector. Polarization on the RFN can be switched from linear to circular,

Table 5.2. Simulated results of the dual-feed CP beam scanning antenna consisting of driven element with one tunable parasitic element.

Capacitance (pF)	θ (degree)	AR (dB)	Gain (dBic)	3-dB beamwidth (degree)	3-dB AR beamwidth (degree)	3-dB AR bandwidth (GHz)
0.84	−14	1.69	2.46	−57-41 (98)	−104-71 (175)	2.28-3.39
1.62	−2	2.03	3.02	−52-40 (92)	−75-74 (149)	2.07-3.55
1.82	4	1.92	3.16	−50-42 (92)	−65-74 (139)	1.74-3.25
2.09	6	1.62	3.40	−42-44 (86)	−46-80 (126)	1.61-3.09
2.41	12	1.32	3.58	−29-47 (76)	−30-80 (110)	1.45-2.85
2.80	18	1.05	3.38	−12-53 (65)	−17-78 (95)	1.41-2.74
3.28	24	1.03	2.51	−5-56 (61)	−9-77 (86)	1.92-2.71
3.95	24	1.02	1.55	−8-58 (66)	−4-76 (80)	1.92-2.68
5.08	24	1.09	0.95	−8-58 (66)	−1-74 (75)	1.88-2.72

by controlling operating states of the RF switches. Output signals of the RFN are represented as output 1 (port 2) and output 2 (port 3). The direction along the x-axis and y-axis is defined as LVP and LHP, respectively. The LVP operating mode is obtained by routing the RF signal through SP4T and SPDT 1 switch. Whereas, the LHP is realized by passing the signal through SP4T and SPDT 2 switch. For the RHCP and LHCP operating mode, the signal passed through the hybrid coupler and distributed into two RF output ports with equal magnitude and $\pm 90^{\circ}$ phase difference. The sense of polarization in CP operating mode can be varied by controlling input given to the hybrid coupler through the SP4T switch.

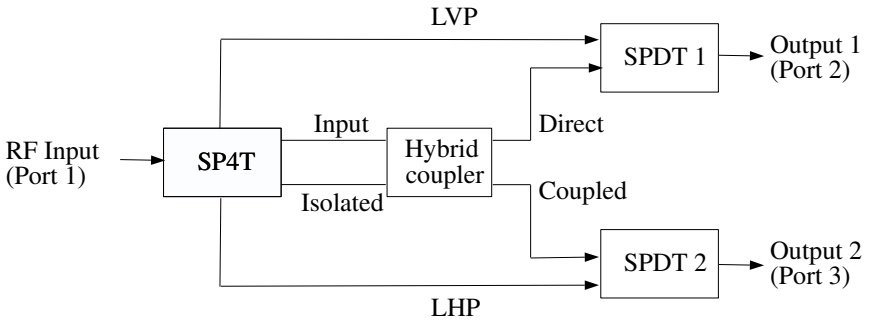

Figure 5.15. Block diagram of the reconfigurable feeding network.

5.2.3.1 3-dB Hybrid Coupler

Figure 5.16 shows schematic of the 3-dB quadrature hybrid coupler which provides good impedance matching, balanced power splitting and consistent 90° phase shifting across a wide bandwidth. Design parameters of the coupler are as follows: Z_0 = 50 Ω, $Z_0/\sqrt{2}$ = 35.35 Ω, L_{50} = 16 mm $\approx \lambda_g/4$, W_{50} = 3 mm, $L_{35.35}$ = 16 mm $\approx \lambda_g/4$ and $W_{35.35}$ = 5 mm. Figure 5.17 depicts a

photograph of the fabricated coupler. The performance of the 3-dB quadrature hybrid coupler is experimentally verified on VNA by terminating unconnected ports with a matched load of 50 Ω. Figure 5.18 presents simulated and measured S-parameter characteristics. The coupler exhibits a measured impedance bandwidth ($S_{11} < -10$ dB) of 58% from 1.8 to 3.3 GHz. It shows balanced output power distribution with S_{21} = −4.09 dB and S_{31} = −4.02 dB over a bandwidth from 2 to 3 GHz. Insertion loss and isolation of the 3-dB quadrature hybrid coupler is −1.09 dB and −18 dB respectively at an operating frequency of 2.45 GHz. The coupler achieves consistent 90° (±10°) output phase difference over a bandwidth from 2 to 3 GHz, as shown in Figure 5.19. The phase difference between two output ports (port 2 and port 3) at 2.45 GHz is found to be 92°.

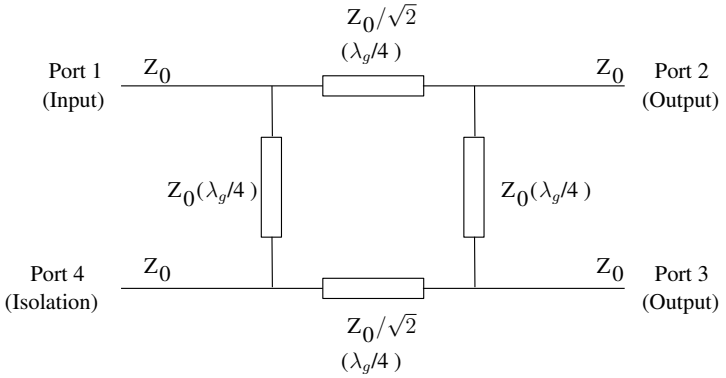

Figure 5.16. Schematic of the 3-dB quadrature hybrid coupler.

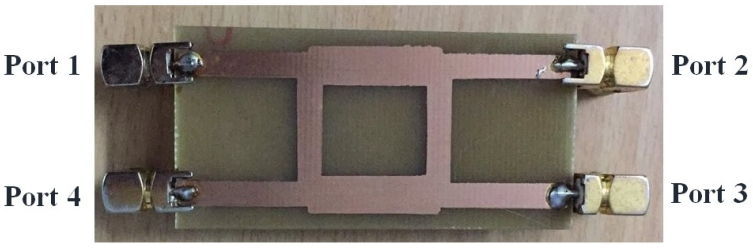

Figure 5.17. Photograph of the fabricated 3-dB quadrature hybrid coupler.

5.2.3.2 Linear Tapered Feed Line

A linear tapered feed line is used to connect pads of the SP4T and SPDT switch to a 50 Ω transmission line. Schematic of the linear tapered feed line is shown in Figure 5.20. Figure 5.21 presents a photograph of the fabricated linear tapered feed line. The gap between two sections of the tapered line can be controlled to attain desired impedance matching by minimizing reflection losses on the transmission line. Simulated and measured reflection characteristics of the tapered feed line are found to be in good agreement. From Figure 5.22, it can be observed that the linear tapered feed line shows good impedance matching with measured −10 dB impedance bandwidth

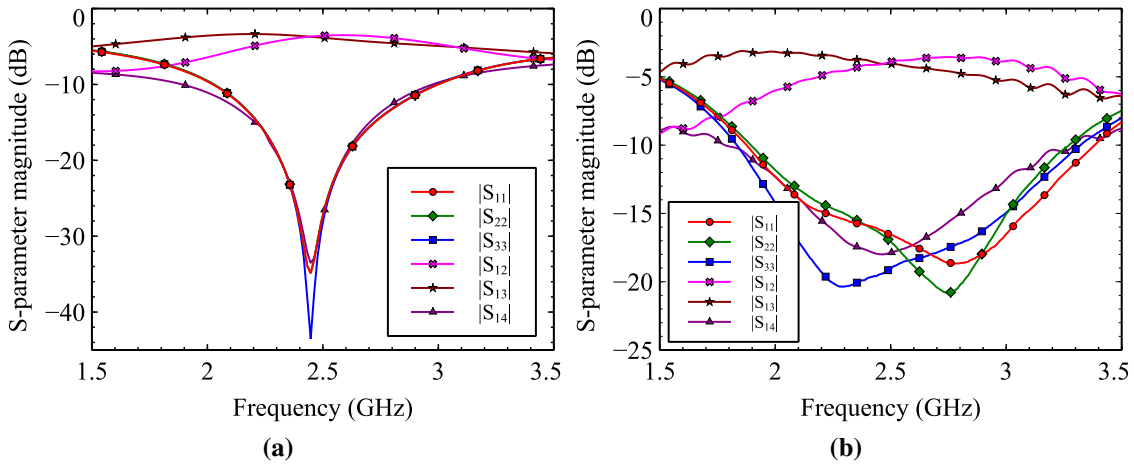

Figure 5.18. S-parameter characteristics of the 3-dB quadrature hybrid coupler (a) Simulated and (b) Measured.

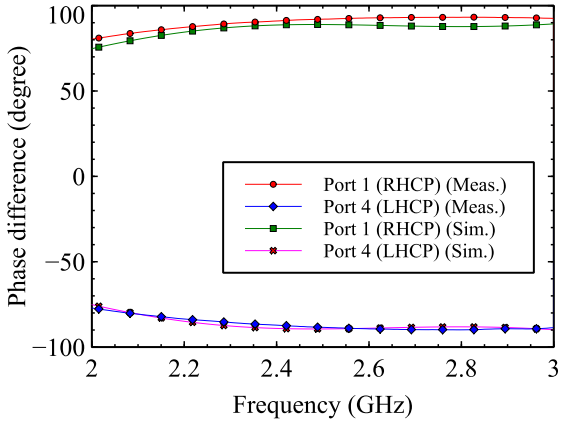

Figure 5.19. Simulated and measured phase characteristics of the 3-dB quadrature hybrid coupler.

from 2 to 3 GHz. The simulated and measured insertion loss at 2.45 GHz is -0.72 and -0.78 dB, respectively. Performance of the transmission line is also experimentally verified by combining linear tapered feed line and 3-dB quadrature hybrid coupler. Figure 5.23 shows a photograph of the fabricated linear tapered feed line with a 3-dB quadrature hybrid coupler. Performance of this configuration is experimentally tested using VNA. Port 1 is connected to the input port of the VNA, while port 4 is terminated with a matched load of 50 Ω. Here, the output ports are represented as port 2 and port 3 respectively. The simulated and measured result shows good matching at all the ports with an overall -10 dB bandwidth from 2.2 to 2.9 GHz. This configuration shows best isolation characteristics with $|S_{23}|$ and $|S_{14}|$ is in the frequency range from 1.9 to 2.9 GHz and 2.2 to 3.3 GHz, respectively. The insertion loss $|S_{12}|$ and $|S_{13}|$ at 2.45 GHz is -1.2 and -1.3 dB respectively. This design shows consistent 90° ($\pm 10°$) phase in the frequency range from 2.3 to 3.2 GHz. The measured phase difference between the two ports is 93° at 2.45 GHz. Detailed simulated and measured results are summarized in Table 5.3.

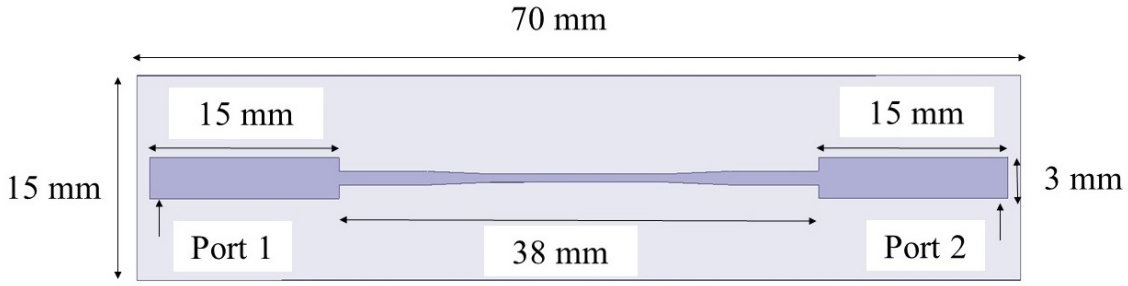

Figure 5.20. Schematic of the linear tapered feed line.

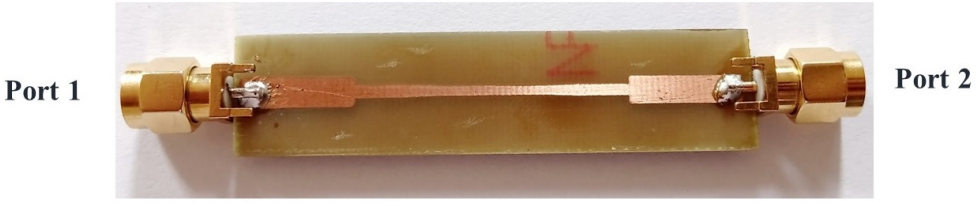

Figure 5.21. Photograph of the fabricated linear tapered feed line.

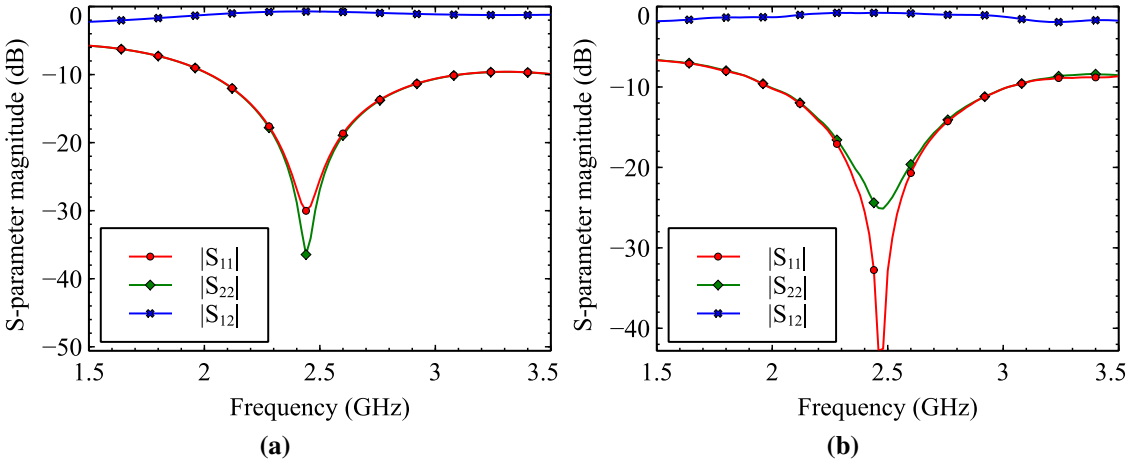

Figure 5.22. S-parameter characteristics of the linear tapered feed line (a) Simulated and (b) Measured.

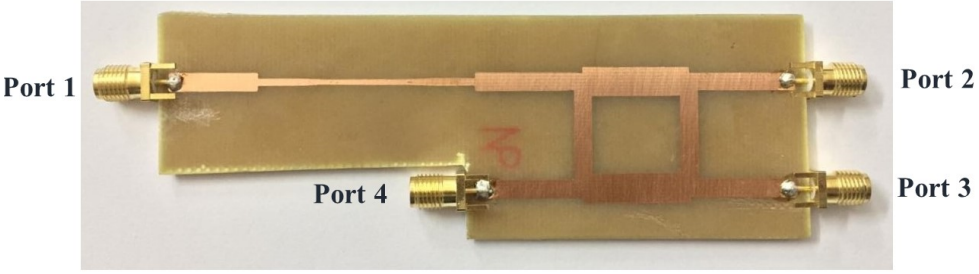

Figure 5.23. Photograph of the fabricated linear tapered feed line with 3-dB quadrature hybrid coupler.

Table 5.3. Simulated and measured results of the linear tapered feed line with 3-dB quadrature hybrid coupler.

Parameter	Simulated	Measured
$\|S_{11}\|$	2.2 to 3.2 GHz	2.2 to 3.3 GHz
$\|S_{22}\|$	1.9 to 2.8 GHz	1.9 to 2.9 GHz
$\|S_{33}\|$	2.1 to 3.1 GHz	2 to 3.3 GHz
$\|S_{23}\|$	2 to 3 GHz	1.9 to 2.9 GHz
$\|S_{14}\|$	1.7 to 3 GHz	2.2 to 3.3 GHz
$\|S_{12}\|$ @ 2.45 GHz	-4.1 dB	-4.2 dB
$\|S_{13}\|$ @ 2.45 GHz	-4.2 dB	-4.3 dB
$\angle S_{12} - \angle S_{13}$ @ 2.45 GHz	89°	93°
$\angle S_{12} - \angle S_{13}$ ($\pm 10°$)	2.3 to 3.2 GHz	2.3 to 3.2 GHz

Figure 5.24 shows a photograph of the fabricated RFN which is designed and developed using FR4 substrate with ϵ_r = 4.3, h = 1.6 mm and $\tan\delta$ = 0.02. The overall size of the RFN is 140×140×1.6 mm^3. Table 5.4 summarizes operating states of the control signals used on the RFN to generate LVP, LHP, LHCP and RHCP operating mode. The control signals of the RF switches SP4T, SPDT 1, and SPDT 2 are represented as (A_1, B_1), (A_2, B_2), and (A_3, B_3) respectively. In the proposed RFN, non-reflective SP4T [162] and SPDT [163] RF switches from Analog Devices are used. The SP4T switch operates in the frequency range from DC to 3.5 GHz. It provides good isolation of 36 dB and insertion loss of -0.7 dB at 2.5 GHz. The SPDT switch operates in the frequency from DC to 4 GHz. It provides high isolation of 52 dB and insertion loss of -0.8 dB at 2.5 GHz. DC voltage to the RF switches is applied using Keithleys programmable DC power supply. Initially, the signal is applied to the port 1 terminal of RFN. Then the signal passes through the SP4T switch, and appropriate polarization mode gets selected. In the RHCP mode of operation, the control signals on the RFN are selected as (A_1, B_1) = (Low, Low). This signal then passed through the 3-dB quadrature hybrid coupler and applied to port 2 and port 3. Based on the control signal inputs on the SPDT 1 and SPDT 2 switch, the equal amplitude and 90° phase difference signal is applied to the port 2 and port 3. Similarly, the other polarization operating modes are selected based on the control signals tabulated in Table 5.4. The functional diagram of the proposed RFN is shown in Figure 5.25.

Table 5.4. Control signals used on the RFN to obtain LVP, LHP, LHCP and RHCP operating state. Here, the Low and High represent 0 V and 5 V respectively.

Polarization mode	SP4T		SPDT 1		SPDT 2	
	A_1	B_1	A_2	B_2	A_3	B_3
Mode 1 LVP (Port 2)	Low	High	High	Low	High	Low
Mode 2 LHP (Port 3)	High	High	High	Low	Low	High
Mode 3 LHCP	High	Low	Low	High	High	Low
Mode 4 RHCP	Low	Low	Low	High	High	Low

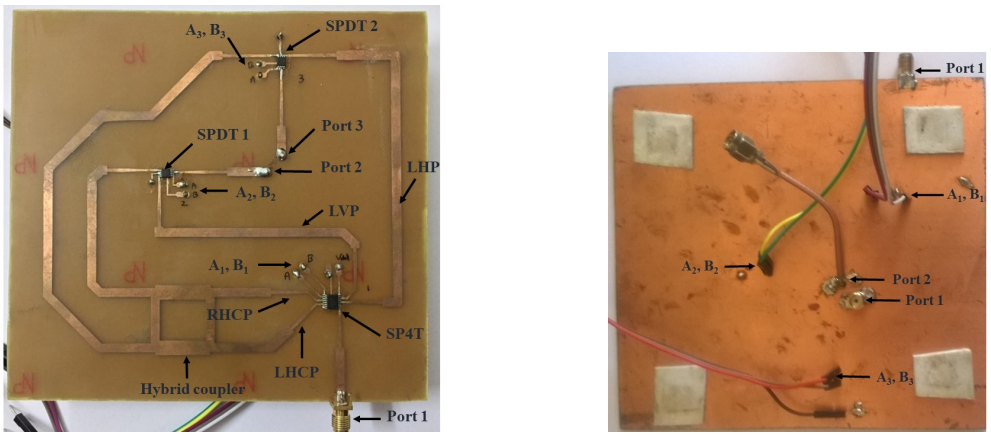

(a) **(b)**

Figure 5.24. Photograph of the fabricated RFN used to produce LVP, LHP, LHCP and RHCP operating states (a) Front view and (b) Back view.

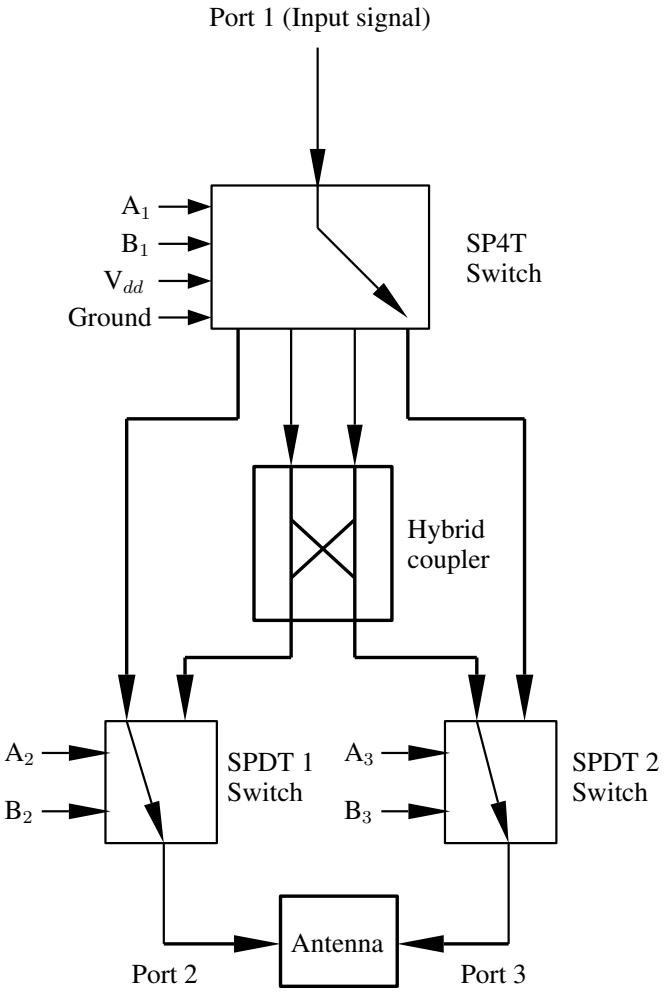

Figure 5.25. Functional block diagram of the RFN.

Figure 5.26 shows S-parameter characteristics for the LP and CP mode of operation. In the LP mode of operation, the RFN shows good impedance matching in the frequency range from 2.2 to 2.8 GHz, and insertion loss at 2.45 GHz is found to be −2.59 dB. For the CP operating mode, output magnitudes $|S_{12}|$ and $|S_{13}|$ are almost equal at 2.45 GHz with $|S_{11}| \leq -10$ dB. The insertion loss for CP mode of operation at 2.45 GHz is −3.59 dB. The insertion loss of LP operating mode includes losses of SP4T switch, one SPDT switch, transmission line, and SMA connector. Whereas, in CP operating mode, the insertion loss of one more SPDT switch is added. The proposed RFN shows phase difference of 90° (±10°) in the frequency range from 2.2 to 2.8 GHz.

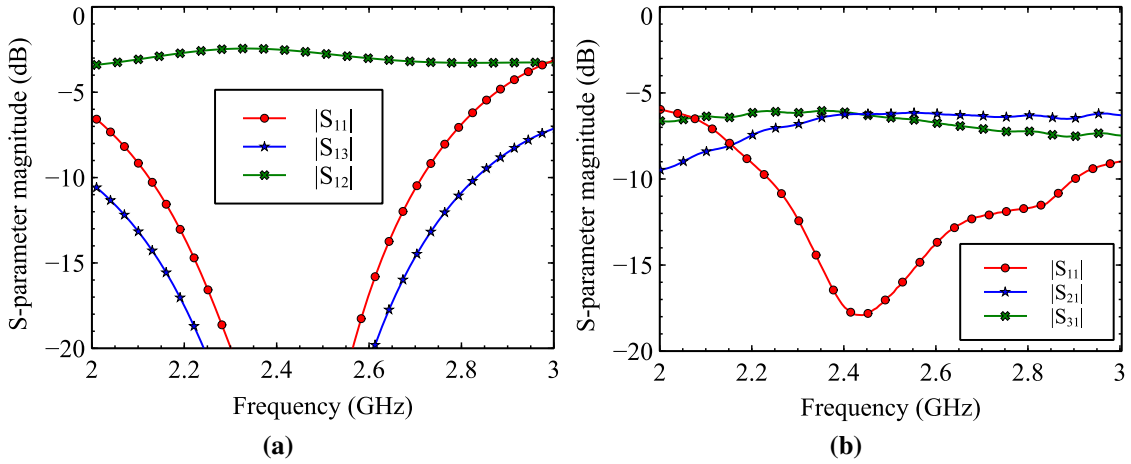

Figure 5.26. Measured S-parameter characteristics of the RFN (a) LP mode and (b) CP mode.

5.3 Results and Discussion

Figure 5.27 shows photographs of the fabricated antenna. The RFN is placed on the backside of the antenna using four wooden supports. The output ports of the dual-feed driven element are connected to input ports of the RFN using 6-inch flexible coaxial cables. The LP is obtained by exciting only one port, while CP is generated by exciting both the input ports with equal magnitude and phase difference of ±90°. Table 5.5 summarizes details of the active components used in the proposed antenna and RFN. Skyworks SMV 1233-079 varactor diodes are used for the practical implementation of the proposed antenna. DC voltage to the cathode terminal of varactor diodes is applied using metallic vias V1, V2, V3, and V4 through Coilcrafts RF choke coil. Anode terminal of the varactor diodes is grounded using metallic vias V5, V6, V7, and V8 placed between the patch layer and ground plane. Two Keithleys programmable DC power supplies are used to apply voltage to the varactor diodes and RF switches. The CP characteristic of the proposed antenna

is measured by using the phase-amplitude method [35]. Performance of the proposed antenna is experimentally tested in the following operating modes: 1) Broadside, 2) Pattern reconfiguration, and 3) Beamwidth reconfiguration. Performance of this antenna is identical in different operating states. For the sake of brevity, simulated and measured results are presented for LVP and RHCP operating mode.

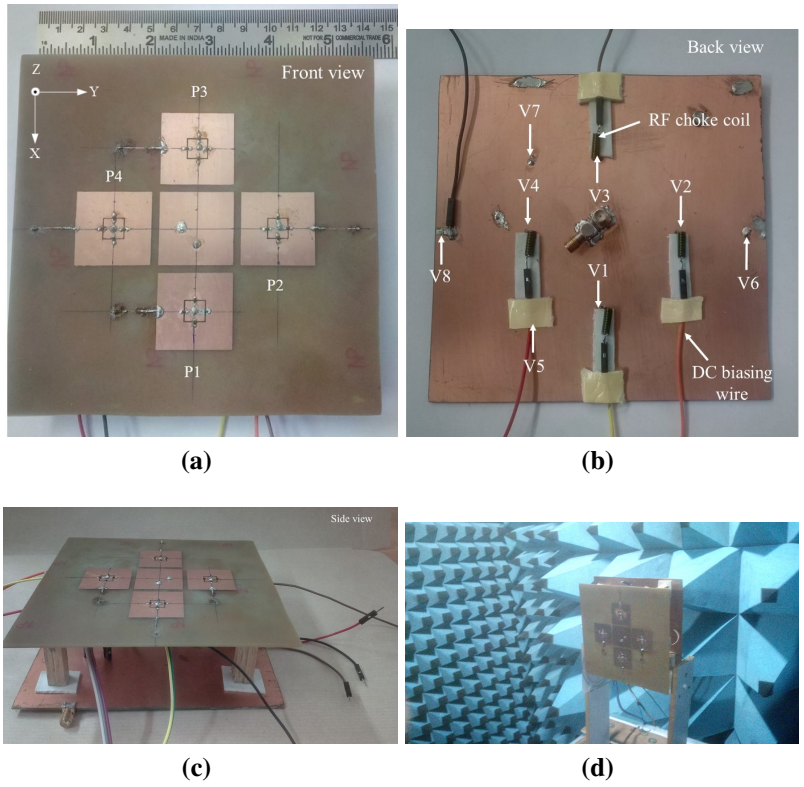

Figure 5.27. Photographs of the fabricated pattern and polarization RA (a) Front view, (b) Back view, (c) Side view and (d) Radiation pattern measurement setup used in the anechoic chamber.

Table 5.5. Details of the active components used in the proposed antenna and RFN.

Component type	Model	Value	Operating frequency	Insertion loss
Varactor diode	SMV 1233-079	0.84 to 5.08 pF	up to 10 GHz	−0.39 to −1.72 dB
RF choke coil	Coilcraft 4310LC-132KEB	1.3 μH	up to 6 GHz	-
SPDT switch	HMC 435AMS8G	-	DC to 4 GHz	−0.8 dB
SP4T switch	HMC 241AQS16	-	DC to 3.5 GHz	−0.7 dB

5.3.1 Broadside Mode

For this mode of operation, all the tunable parasitic patch P1, P2, P3, and P4 capacitance values are set at 1.82 pF. The simulated and measured reflection characteristics are shown in the Figure 5.28. Figure 5.29 shows normalized simulated and measured far-field radiation pattern in the E-plane and H-plane for LVP operating state. It is observed that antenna radiates in broadside direction with a measured peak gain of 2.35 dBi. The measured 3-dB beamwidth in the E-plane and H-plane is 99° and 81°, respectively. For the RHCP mode of operation, the antenna produces a broadside radiation pattern in both the planes with 3-dB coverage of 87°, as shown in Figure 5.30. The measured gain of the antenna is found to be 2.24 dBic. The measured AR in both the planes for θ = 0° direction is 0.60 dB and 0.51 dB respectively. The measured 3-dB AR beamwidth in the ϕ = 0° plane and ϕ = 90° plane is $-49°$ to 47° and $-34°$ to 50° respectively.

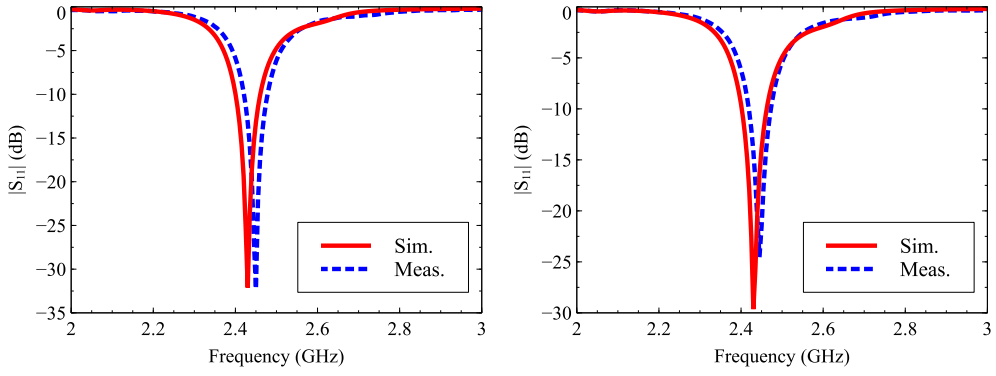

Figure 5.28. Simulated and measured reflection characteristics in the broadside mode (a) LVP and (b) RHCP.

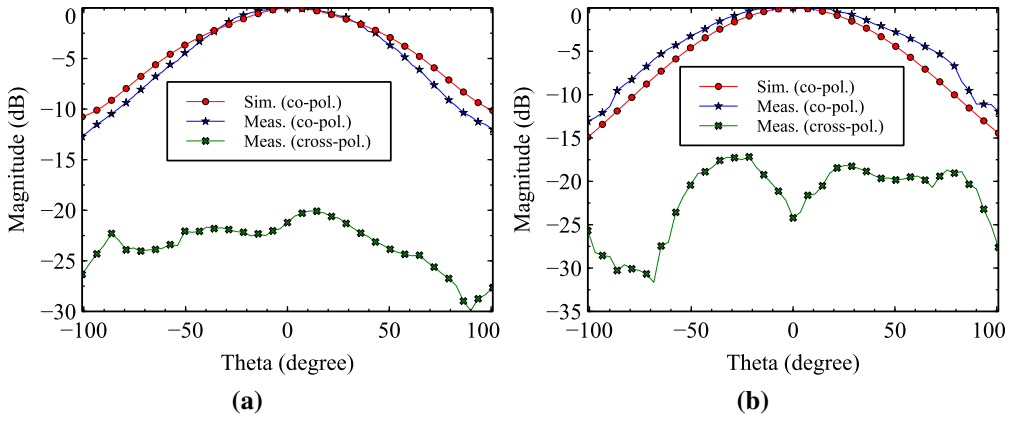

Figure 5.29. Normalized simulated and measured far-field radiation pattern in the broadside mode at 2.45 GHz with LVP (a) ϕ = 0° plane (xz-plane) and (b) ϕ = 90° plane (yz-plane).

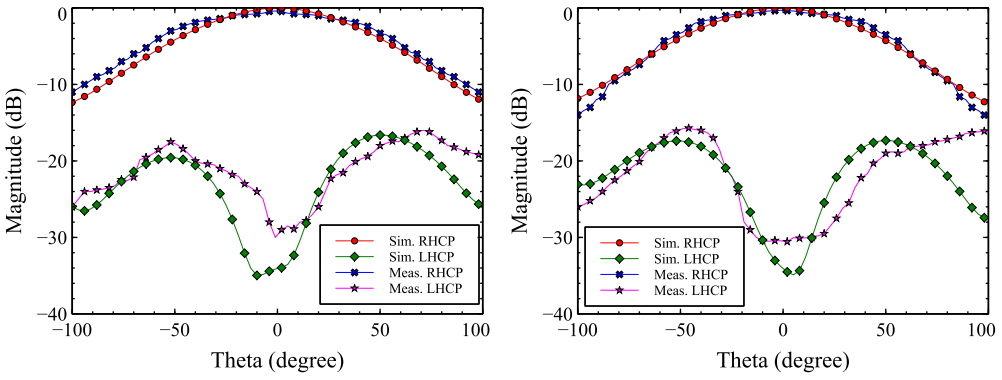

Figure 5.30. Normalized simulated and measured far-field radiation pattern in the broadside mode at 2.45 GHz with RHCP (a) $\phi = 0°$ plane (xz-plane) and (b) $\phi = 90°$ plane (yz-plane).

5.3.2 Pattern Reconfiguration

This section presents simulated and measured results obtained in the LVP and RHCP operating mode with pattern reconfiguration. The continuous beam scanning results with LVP and RHCP operating mode are experimentally verified in three planes $\phi = 0°$, $45°$ and $90°$. Similar performance can be obtained in $\phi = 135°$, $180°$, $225°$, $270°$, $315°$ planes by properly selecting tunable parasitic patch capacitance values. The tunable parasitic patch capacitance values used in the different planes to achieve continuous beam scanning with LP and CP configuration are summarized in Table 5.6 and Table 5.7.

Table 5.6. Tunable Parasitic capacitance values used in $\phi = 0°$, $45°$ and $90°$ planes to achieve continuous beam scanning with LP configuration.

Plane	P1 (pF)	P2 (pF)	P3 (pF)	P4 (pF)
$\phi = 0°$ (xz-plane)	2.09 - 2.8	1.82	0.84	1.82
$\phi = 45°$	2.09 - 5.08	2.09 - 5.08	1.82	1.82
$\phi = 90°$ (yz-plane)	1.82	1.62 - 5.08	1.82	0.84

Table 5.7. Tunable Parasitic capacitance values used in $\phi = 0°$, $45°$ and $90°$ planes to achieve continuous beam scanning with CP configuration.

Plane	P1 (pF)	P2 (pF)	P3 (pF)	P4 (pF)
$\phi = 0°$ (xz-plane)	1.62 - 5.08	1.82	0.84	1.82
$\phi = 45°$	2.09 - 5.08	2.09 - 5.08	1.82	1.82
$\phi = 90°$ (yz-plane)	1.82	1.62 - 5.08	1.82	0.84

5.3.2.1 Linear Vertical Polarization (LVP) State

The simulated and measured reflection coefficient in the different operating planes is shown in Figure 5.31. Figure 5.32 shows normalized simulated and measured far-field radiation patterns at 2.45 GHz. The main beam of antenna is continuously scanned in the $\phi = 0°$ plane from 2° to 11°, as the capacitance is varied from 2.09 to 2.8 pF. Peak gain of antenna varies from 2.21 to 2.98 dBi with 3-dB coverage from $-43°$ to 65°. In $\phi = 45°$ plane, the radiated beam is continuously scanned from 0° to 32° with gain variation from 0.50 to 2.90 dBi. The 3-dB beamwidth ranges from $-37°$ to 65°. In $\phi = 90°$ plane, the parasitic elements P2 and P4 placed in the H-plane are used as reflector and director respectively. The capacitance of P1 and P3 parasitic element placed in the E-plane is fixed at 1.82 pF. Main beam of the antenna in this plane is continuously scanned from 5° to 40°, as the capacitance is varied from 1.62 to 5.08 pF. The Peak gain of the antenna varies from 0.20 to 2.32 dBi. The 3-dB beamwidth of antenna ranges from $-46°$ to 71°.

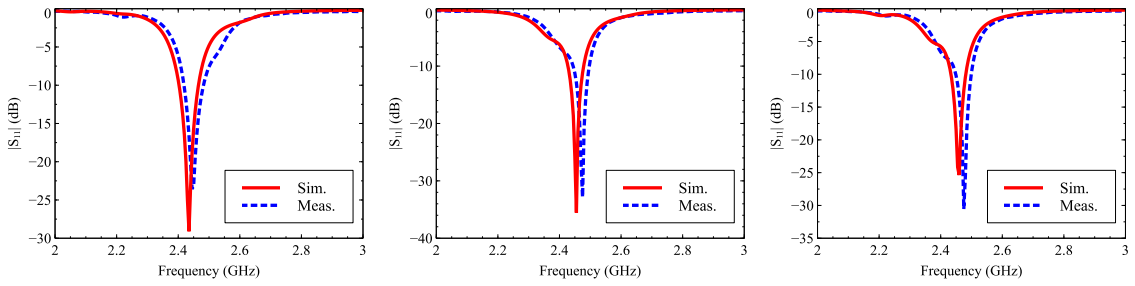

Figure 5.31. Simulated and measured reflection characteristics in the LVP pattern reconfiguration mode (a) 2.8 pF ($\phi = 0°$), (b) 5.08 pF ($\phi = 45°$) and (c) 5.08 pF ($\phi = 90°$).

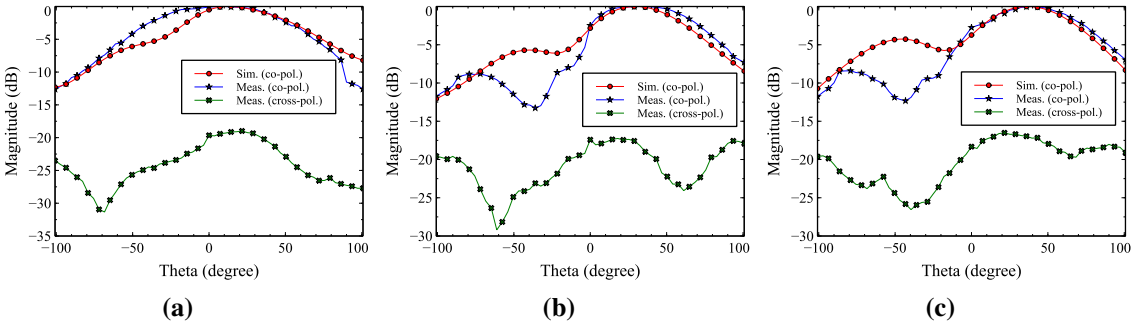

Figure 5.32. Normalized simulated and measured far-field radiation pattern with LVP at 2.45 GHz (a) 2.8 pF ($\phi = 0°$), (b) 5.08 pF ($\phi = 45°$) and (c) 5.08 pF ($\phi = 90°$).

5.3.2.2 Right-Hand Circular Polarization (RHCP) State

In this mode, results obtained for continuous beam scanning with RHCP are described in xz-plane, 45° plane, and yz-plane. The simulated and measured reflection characteristics for this mode of operation are shown in Figure 5.33. Figure 5.34 shows the normalized simulated and measured far-field radiation pattern at 2.45 GHz in all the three operating planes for capacitance 5.08 pF. In xz-plane, the main beam of antenna is continuously scanned from 2° to 30° with a gain variation from 0.54 to 2.78 dBic, as the capacitance of P1 parasitic element is varied from 1.62 to 5.08 pF. The 3-dB beamwidth of the antenna ranges from −46° to 71°. It is observed that the AR is less than 3 dB in all the beam scanning directions, and it ranges from 0.35 to 2.60 dB for the capacitance range from 1.62 to 5.08 pF. Minimum AR of 0.35 dB is obtained for the capacitance 2.09 pF when the main beam is steered to 8°. In $\phi = 45°$ plane, the main beam is continuously scanned from 0° to 30° with gain variation from 0.15 to 3.12 dBic. Overall 3-dB beamwidth ranges from −40° to 62°. The AR in the main beam scanned direction is found to be in the range of 0.34 to 2.28 dB. In the yz-plane, a radiated beam is continuously scanned from 2° to 30°. Over the beam scanning range gain of the antenna varies from 0.31 to 2.54 dBic. The 3-dB beamwidth of the antenna is found to be in the range of −49° to 68°. The AR in beam scanning direction varies from 0.65 to 2.81 dB. The measured 3-dB AR beamwidth decreases from 96° to 15°, as the main beam is scanned from 2° to 30°. From Figure 5.35, it can be seen that the proposed antenna shows a 3-dB AR bandwidth from 2.43 to 2.48 GHz in the yz-plane for capacitance 5.08 pF.

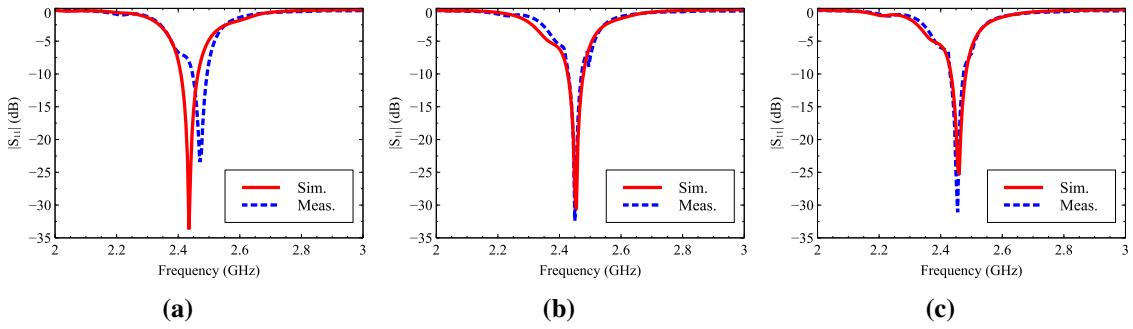

Figure 5.33. Simulated and measured reflection characteristics in the RHCP pattern reconfiguration mode (a) xz-plane, (b) $\phi = 45°$ plane and (c) yz-plane.

5.3.3 Beamwidth Reconfiguration

Beamwidth of the proposed RA can be continuously tuned either individually or simultaneously in the E-plane and H-plane. In all these planes, the antenna shows unidirectional radiation characteristics with the main beam directed in broadside direction. The overall −10 dB impedance

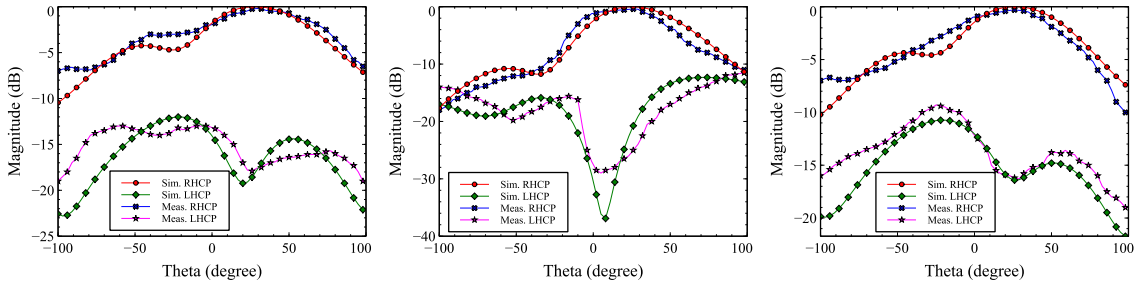

Figure 5.34. Normalized simulated and measured far-field radiation pattern with RHCP at 2.45 GHz for capacitance 5.08 pF (a) xz-plane, (b) $\phi = 45°$ plane and (c) yz-plane.

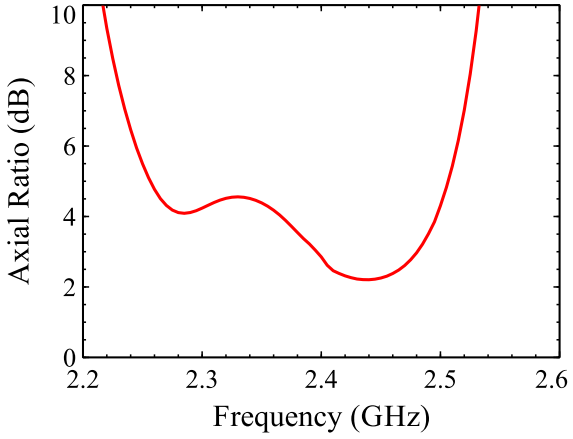

Figure 5.35. Simulated AR bandwidth in the yz-plane for capacitance 5.08 pF.

bandwidth in all the operating planes is found to be from 2.43 to 2.47 GHz. Tunable parasitic patch capacitance values used for beamwidth reconfiguration in three different operating modes are summarized in Table 5.8. Here, the measured beamwidth reconfiguration results are shown for LVP mode. Tunable beamwidth can be obtained with LHP mode by properly selecting control signals on the RFN.

Table 5.8. Capacitance values used in the E-plane and H-plane to obtain individual as well as simultaneous beamwidth reconfiguration.

Plane	P1 (pF)	P2 (pF)	P3 (pF)	P4 (pF)
E-plane (Individual)	0.84 - 5.08	1.82	0.84-5.08	1.82
H-plane (Individual)	1.82	0.84 - 2.8	1.82	0.84 - 2.8
E-plane & H-plane (Simultaneous)	0.84 - 2.8	0.84 - 2.8	0.84 - 2.8	0.84 - 2.8

In E-plane, the 3-dB beamwidth is continuously tuned from 66° to 152° with average H-plane beamwidth of 80°. Figure 5.36(a) shows measured tunable beamwidth characteristics in the E-plane for capacitance from 0.84 and 5.08 pF. The measured result shows that excellent impedance matching is observed at all the capacitance values with -10 dB bandwidth from 2.41

to 2.47 GHz. The antenna achieves a narrow beamwidth of 66° at 2.8 pF and a wide beamwidth of 152° at 5.08 pF. Over the beamwidth tuning range, peak gain and directivity of the antenna varies from 0.13 to 3.09 dBi and 5.86 to 8.04 dB, respectively. Similarly, the individual beamwidth reconfiguration in the H-plane is obtained by varying the capacitance of tunable parasitic elements P2 and P4 from 0.84 to 2.8 pF. The capacitance of tunable parasitic elements P1 and P3 placed in the E-plane is fixed at 1.82 pF. The antenna shows −10 dB impedance bandwidth from 2.42 to 2.47 GHz for the capacitance range from 0.84 to 2.8 pF. Desired impedance characteristics are not obtained for the capacitance range from 3.28 to 5.08 pF due to the strong mutual coupling between driven and tunable parasitic elements placed in the H-plane. The 3-dB beamwidth in the H-plane is continuously tuned from 60° to 108° with average E-plane beamwidth of 90°, as shown in Figure 5.36(b). The measured gain and simulated directivity are in the range of 0.38 to 2.89 dBi and 6.53 to 7.74 dB, respectively. To achieve simultaneous beamwidth reconfiguration, capacitance on the tunable parasitic elements P1, P2, P3, and P4 is continuously varied from 0.84 to 2.8 pF. Reflection characteristics show excellent impedance matching with overall −10 dB impedance bandwidth from 2.43 to 2.47 GHz. Figure 5.37 shows the beamwidth reconfiguration characteristics with simultaneous variation in E-plane and H-plane. The 3-dB beamwidth is continuously tuned from 78° to 120° and 57° to 120° in the E-plane and H-plane respectively. The peak gain and directivity are found to be in the range of 0.24 to 2.74 dBi and 5.65 to 8.52 dB respectively.

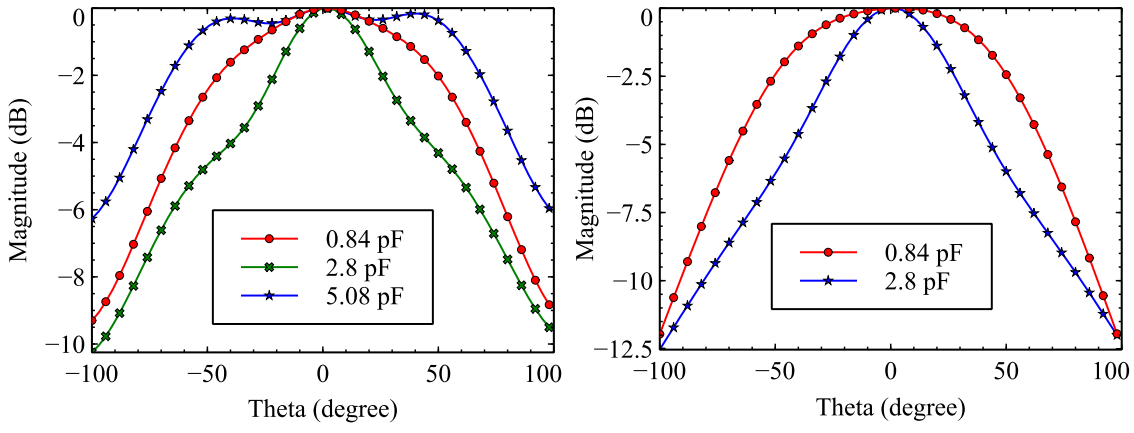

Figure 5.36. Measured individual beamwidth reconfiguration at 2.45 GHz (a) E-plane and (b) H-plane.

5.3.4 Performance Comparison

Table 5.9 presents a detailed performance comparison of the proposed RA with other reported designs in the literature, achieving pattern reconfiguration with LP as well as CP. The proposed

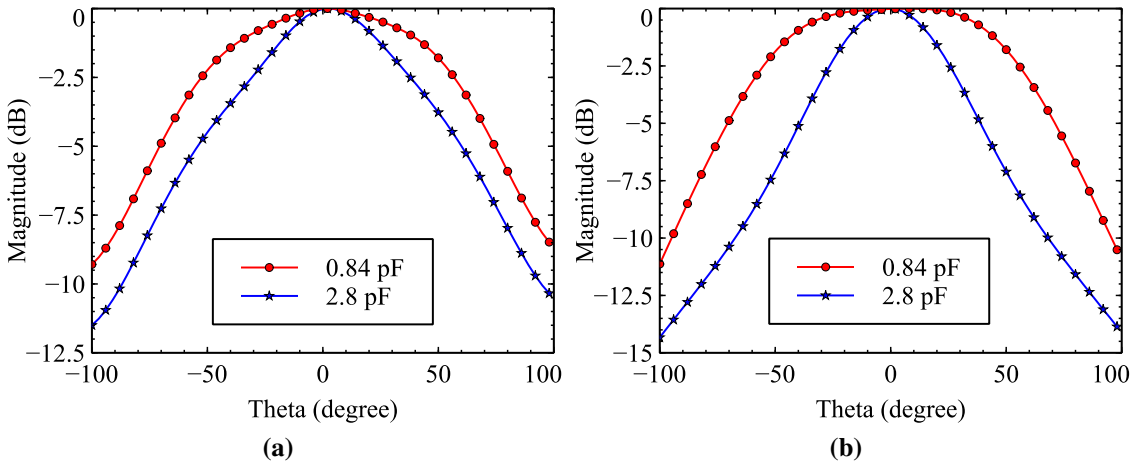

Figure 5.37. Measured simultaneous beamwidth reconfiguration at 2.45 GHz (a) E-plane and (b) H-plane.

antenna overcome limitations of the reported designs with respect to limited 360° coverage in the azimuth plane [15, 140–144, 147] and discrete beam switching in [15, 140–145, 147]. It is noted that the design presented in [143, 144] are unable to attain independent pattern and polarization reconfiguration. In [15], independent pattern and polarization is realized with the main beam is discretely switched to 30° in the elevation plane. However, this antenna needs 60 PIN diodes, which increases the power consumption and complicates the DC biasing network. Also, the beam steering is achieved in two principal planes, and complete 360° azimuth coverage is not obtained. RA design presented in [147] achieves limited beam switching of ±20° with LP. In LHCP and RHCP operating mode, beam steering is not obtained and the main beam is radiated in the broadside direction. It can be seen that the proposed RA can provide the independent pattern, polarization, and beamwidth reconfiguration in a single antenna structure. In all the other reported pattern and polarization RA designs, beamwidth reconfiguration is not realized.

5.4 Summary

Reconfigurable antenna design is proposed to achieve independent pattern and polarization reconfiguration along with beamwidth variability. The proposed antenna consists of a square-shaped driven element and four varactor loaded parasitic elements placed in the E-plane and H-plane. The RFN consisting of a 3-dB quadrature hybrid coupler, one SP4T switch, and two SPDT switches is developed to obtain LVP, LHP, LHCP, and RHCP operating states. In each polarization state, the main beam of the antenna is independently continuously scanned in the elevation plane and covers a complete azimuth plane. Moreover, 3-dB beamwidth of this antenna

Table 5.9. Performance comparison of the proposed pattern and polarization RA with other reported designs.

Ref.	Operating frequency (GHz)	360° azimuth coverage	Main beam elevation plane (degree)	Polarization	Peak gain	Switches (number)	Steering type	Beamwidth reconfi-gurability
[140]	10.3	no	broadside, 4, ±19, ±10	LP LHCP	n/a	copper strips (8)	discrete	no
[141]	5.25	no	−30, 0, 30	LP, CP	8	copper strips (40)	discrete	no
[142]	1.57	no	±15 ±25 L 30, R −30	LP LP LHCP, RHCP	4.2	PIN (4)	discrete	no
[143]	5.2 5.8	no	±30	±45 LP, LHCP, RHCP	3	PIN (6)	discrete	no
[144]	3.6 5.8	no	omni broadside broadside, ±30 broadside	LP LHCP LP RHCP	8.9	PIN (10)	discrete	no
[145]	4.02	yes	≈35	LVP, LHP LHCP, RHCP	8.68	copper strips (12)	discrete	no
[15]	2.7	no	±30	LVP, LHP LHCP, RHCP	4 dB (avg.)	PIN (60)	discrete	no
[147]	3.3	no	±20 broadside	LP LHCP, RHCP	n/a	PIN (12)	discrete	no
Proposed	2.45	yes	11 (E-plane) 40 (H-plane) 30	LVP, LHP LHCP, RHCP	3 (avg.)	varactor (16)	continuous	yes

can also be continuously tuned in E-plane, H-plane, and both E-plane and H-plane with LVP and LHP operating states.